

Measuring Light Echos in NGC 4051

T. J. Turner¹, L. Miller², J.N.Reeves^{3,4}, V.Braito^{3,5}

¹*Dept. of Physics, University of Maryland Baltimore County, Baltimore, MD 21250, U.S.A.*

²*Dept. of Physics, Oxford University, Denys Wilkinson Building, Keble Road, Oxford OX1 3RH, U.K.*

³*Center for Space Science and Technology, University of Maryland Baltimore County, 1000 Hilltop Circle, Baltimore, MD 21250, USA*

⁴*Astrophysics Group, School of Physical and Geographical Sciences, Keele University, Keele, Staffordshire ST5 5BG, U.K*

⁵*INAF-Osservatorio Astronomico di Brera, Via Bianchi 46, I-23807 Merate (LC), Italy*

Accepted 2016. Received 2016; in original form 2016

ABSTRACT

We have analyzed five archived X-ray observations of NGC 4051 taken using the *NuSTAR* observatory. The data show lags between flux variations in bands of different X-ray photon energy. In all pairs of bands compared, the harder band consistently lags the softer band by at least 1000 s, at temporal frequencies $\sim 5 \times 10^{-5}$ Hz. In addition, soft-band lags up to 400 s are measured at temporal frequencies $\sim 2 \times 10^{-4}$ Hz. Light echos from the inner accretion disk cannot explain the lags in these data, as a sharp soft-band lag is seen in cross-correlations where the softer band is expected to have no contribution from reflection. We find a simple top hat model to be consistent with the response function producing the reprocessed signal. The scattered fraction of X-rays is high, indicating the reprocessor to have a global covering fraction $\sim 50\%$ around the continuum source. The scattered fraction increases with increasing photon energy, while the maximum time delay decreases. Such a scenario may be explained by a higher fraction of the soft photons being scattered from large radii relative to the hard photons. A stratified clumpy wind provides a compelling physical model that satisfies all observational criteria.

Key words: galaxies: active - X-rays: galaxies - accretion, accretion disks - galaxies: individual: NGC 4051

1 INTRODUCTION

Variations in X-ray flux are common in Active Galactic Nuclei (AGN), where factors of several change are evident over all timescales observed, ie. from tens of seconds to years. Interpretation of the flux variations and the dependences on photon energy may allow insight into the physical processes that are important in the immediate neighborhood of the supermassive nuclear black hole. Construction of a power spectral density (PSD) can help characterize the variations, showing the relative importance of the different temporal modes sampled by the data, while the lag spectrum shows the time lags between two light curves extracted from different energy ranges; these are analyzed as a function of the frequency of Fourier modes (convention defines a positive lag as hard photons lagging soft).

Time delays are expected to arise from reverberation in the X-ray band, caused by reprocessing and scattering of the continuum radiation by circumnuclear material. Of particular interest is the so-called transfer function, that is a measure of the time delays between time series constructed in differing bands of X-ray photon energy, analyzed as a function of the temporal frequency of modes of variation. Energy- and frequency-dependent time delays appear

to be a common feature of the X-ray emission from AGN (e.g. [De Marco et al. 2013](#)).

There are currently two principal mechanisms that have been invoked in the literature to explain time delays between X-ray energy bands. The first of these is time delays that may be associated with the possible inwards propagation of fluctuations on the accretion disk (e.g. [Kotov et al. 2001](#); [Arévalo et al. 2006](#)). The inner accretion disk is thought to be hotter than the outer disk, so a delayed fluctuation arriving at the inner disk may stimulate harder X-ray emission than would be produced at larger radii, leading to an energy-dependent time delay of hard photon flux variations lagging soft photon flux variations. However, while this model may work well for X-ray binaries with their hotter accretion disks, in AGN the observed X-ray emission is not thought to arise directly from the disk, as the disk should be too cool. Instead, it is commonly supposed that disk photons are Compton upscattered in energy in a hot corona, of unknown geometry ([Haardt & Maraschi 1991](#)). However, in order to produce the observed powerlaw X-ray spectrum, the optical depth to Compton scattering must be sufficiently high that memory of the input spectrum is largely lost ([Titarchuk 1994](#)) - thus it seems likely that this model needs to assert that coronal fluctuations may produce the require spectral-dependent time de-

lays. It is also commonly supposed that the X-ray source is a compact region close to the black hole event horizon, in order to create a high equivalent width of strongly redshifted Fe K line emission (Miniutti & Fabian 2004). However, if the coronal size is too small then there is no clear mechanism for the inwards disk fluctuations to be transferred into a change in the X-ray emission via the corona: the corona has to be extended in order for the inwards propagation model to work. Despite these difficulties, the ‘propagation of fluctuations’ model remains a popular choice in the literature (Uttley et al. 2014).

The second possible mechanism supposes that time delays arise from light travel time delays, arising when X-ray photons Compton scatter from circumnuclear material. Such a mechanism has been invoked to explain either short timescale delays in AGN (e.g. Fabian et al. 2009) or the entire transfer function of delays across all timescales (e.g. Miller et al. 2010a). These possibilities will be discussed later in this paper in the context of new observations of the nearby AGN NGC 4051.

In the context of reverberation models, the delayed signal, or “light echo” arises from scattering of the X-ray continuum from absorbing circumnuclear or accretion disk material - a process commonly known as ‘reflection’ in the case of optically-thick material. The reverberation component is expected to have a hard spectrum relative to the primary continuum and the contribution of reflection increases with energy. An observed time series generally comprises both direct emission and delayed, scattered emission, so that the net observed reverberation time delay is diluted according to the fraction of direct light that is present. In the harder energy bands the contribution of delayed emission increases and observed time lag tends towards an undiluted value (Miller et al. 2010a). Reverberation models predict we should see a strong delayed signal in the hard X-ray band, peaking above 10 keV.

Owing to low sensitivity, lack of spatial resolution and high background levels, there has been no mission prior to *NuSTAR* that has allowed useful reverberation analysis above 10 keV. Early results show the value of *NuSTAR* in X-ray reverberation analysis. Zoghbi et al. (2014) presented the first analysis of high-frequency time lags in *NuSTAR* data above 10 keV, showing the Compton hump to lag the continuum variations by 1–2 ks in MCG–5-23-16. Kara et al. (2015) claimed a similar result for SWIFT J2127.4+5654 and NGC 1365. Emission from around Fe K α was also found to lag the continuum in all three sources.

This work presents a study of the timing and spectroscopic properties of NGC 4051, observed in five *NuSTAR* observations. In Section 2 we discuss recent analyses of X-ray observations of NGC 4051. In Section 3, we describe the *NuSTAR* data reduction. In Section 4 we present the spectral analysis of the source. In Section 5 we describe our timing analysis methods and in Section 6 we discuss the results in the context of a light echo model for the X-ray reprocessor.

2 NGC 4051

NGC 4051 is a bright, nearby narrow-line Seyfert 1 AGN with low black hole mass, ($M \simeq 1.7 \times 10^6 M_\odot$; Denney et al. 2010) and high accretion rate ($\sim 10\%$ of Eddington), making it one of the most variable Seyfert galaxies in the X-ray band, with factors up to 15 observed on timescales of tens of ks (Ponti et al. 2006). The X-ray spectrum has been well studied and shows a multi-phase outflow, with zone velocities ranging from a few hundred to few thousand km/s, (Pounds et al. 2004a). The ionization of some of the absorb-

ing zones has been observed to change in response to the varying continuum (Lobban et al. 2011; Krongold et al. 2007). The strong and persistent reprocessing signatures show that there is a large amount of circumnuclear material in NGC 4051, making this an ideal target for a detailed reverberation study.

Outflowing reprocessor zones with velocities $50 - 400 \text{ km s}^{-1}$ are also detected in UV spectroscopy of this source (Kaspi et al. 2004). These fit well into the Krongold et al. (2007) picture of an absorbing multi-phase wind and it may be that a significant part of the observed reflection comes from such a wind (Turner et al. 2007). The X-ray continuum itself varies by up to a factor 15 on timescales as short as 20 ks (Ponti et al. 2006). In its low state OVII and OVIII emission lines from distant photoionized gas are prominent (Pounds et al. 2004b; Ponti et al. 2006) and there is likely also a component of distant neutral reflection (Ponti et al. 2006). Ionised Fe X emission is also detected optically up to 150 pc from the central source (Nagao et al. 2000). In summary, the reprocessed spectrum for NGC 4051 appears to include contributions from the inner accretion disk, the broad-line region and from more distant dusty regions of circumnuclear gas.

To study the temporal behaviour of the X-ray emission, McHardy et al. (2004) combined 6.5 years of observations by *RXTE* with a long observation by *XMM-Newton* (hereafter *XMM*), finding the lag of hard X-ray fluctuations to increase and coherence to decrease as band separation increases. They also found the lag and coherence to be greater for variations of longer time period. This behaviour suggested higher photon energies and shorter variability timescales to be associated with smaller radii.

Miller et al. (2010a) presented two long *Suzaku* exposures of NGC 4051, finding a strong hard component above 10 keV, some fraction of which varies with the power-law continuum. The power spectrum was non-stationary, showing differences between the low and high flux states. This was confirmed in *XMM* observations by Alston et al. (2013), who also measured negative time lags and found that the shape of the lag spectra depends on source flux. Frequency-dependent positive time lags $970 \pm 225 \text{ s}$ were measured by Miller et al. (2010a) and suggested to be explained by the effects of reverberation in the hard band, caused by reflection from a thick shell of material with maximum lags of about 10,000s. The reflecting material must extend to a distance of about $1.5 \times 10^{14} \text{ cm}$, i.e. 600 gravitational radii from the illuminating source with high global covering factor ($C_g > 0.44$). The reflection may occur from Compton thick parts of the disk wind, seen out of the line-of-sight. These very long lags in the hard band also exclude the possibility that the hard component originates as reflection from the inner accretion disk in NGV 4051 Miller et al. (2010a).

3 ANALYSIS OF THE NUSTAR DATA

NuSTAR observed NGC 4051 during five observations spread over 2015 May 15 – 22, with exposure times between 9.4 – 56.7 ks (Table 1). The data from both focal plane modules (FPMA and FPMB) and for all observations were reprocessed and cleaned using the most recent version of the *NuSTAR* pipeline (within HEASOFTv16.6) and calibration files (CALDB version 20140715), resulting in 172 ks of good on-source exposure (Table 1).

We extracted spectra and light curves from a circular region of $30''$ radius, centered on the nucleus. Background spectra and light curves were extracted from two circular regions that are free of any obvious point sources and the ratio of source to background areas for the extraction cells was 1:5.5.

Table 1. Observation Log

Date	Observation	Exposure	ct/s 2-10 keV	ct/s 10-50 keV	flux 2-10 keV	flux 10-50 keV
2013-06-17 16:41:07	60001050002	9.4	0.25	0.11	1.99	3.79
2013-06-17 21:21:07	60001050003	45.7	0.25	0.11	1.80	3.17
2013-10-09 13:41:07	60001050005	10.2	0.19	0.09	1.31	2.89
2013-10-09 20:01:07	60001050006	49.6	0.13	0.07	0.93	2.29
2014-02-16 13:36:07	60001050008	56.7	0.35	0.13	2.99	4.19

Note. — Observed fluxes are given for FPMA in units $10^{-11} \text{ erg cm}^{-2} \text{ s}^{-1}$

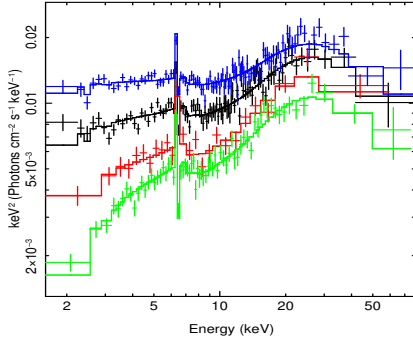


Figure 1. *NuSTAR* data for NGC 4051 - for clarity, only FPMA data are shown. Spectral variability is dominated by changes in the continuum level that drive lagged changes in scattered light. Observations correspond to the colored lines as: 02+03 (black), 05 (red), 06 (green) and 08 (blue) – see Table 2

NGC 4051 shows strong X-ray variability across the observation set (Table 1 and Fig 1). The background is 0.5-2% of the total cts in the 2-70 keV band, 2-5% in the 10-70 keV band. There is no concern regarding dead time in this count rate regime (Table 1).

Examination of the background-subtracted light curves reveals strong time variability within all of the observations (Fig 1). As observations 60001050002 and 60001050003 are very close in count rate and spectral shape and were taken close together in time, we combine those exposures into a single spectrum for the spectral analysis (Table 2).

The spectral data from those summed observations, plus spectra from the other three observations were fit for modules FPMA and FPMB simultaneously. The calibration offset recommended between those two instruments is in the range 0.95-1.05, and so a constant component was allowed in the model, linked to be a single floating value that we fit to obtain a cross-normalization constant 1.05 between the two FPM instruments.

4 SPECTRAL FITTING

To remain within the well-calibrated regime for *NuSTAR*, this paper restricts consideration of spectral data to the $\sim 2 - 70$ keV band. We rebin the spectral data first to 1024 channels to reduce the spectral oversampling, then apply a grouping to achieve a minimum of 20 photons per energy channel in order to facilitate the use of χ^2 statistics. Models were fit to the data using the software package XSPEC ver. 12.9.0 (Arnaud 1996). All models included the Galactic line-of-sight absorption, $N_{\text{H,Gal}} = 1.35 \times 10^{20} \text{ cm}^{-2}$ (Dickey & Lockman 1990), although this had a negligible effect on the fit parameters owing to the spectral cut-off being relatively high, at 2 keV. All model components were adjusted to be at the redshift of

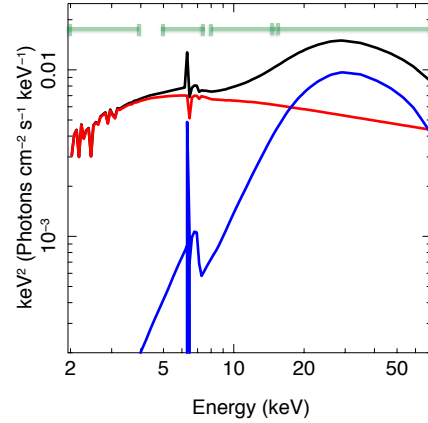


Figure 2. The mean model for NGC 4051 with the boundaries shown for the bands chosen for timing analysis shown as green horizontal lines. The mean powerlaw component is shown in red, the mean scattered component is shown in blue. Both components are modified by a layer of ionized gas and the summed model is shown as a black line.

the host galaxy, except for the Galactic absorption. In the following, unless otherwise stated, fit parameters are quoted in the rest-frame of the source and errors are at the 90% confidence level for one interesting parameter ($\Delta\chi^2 = 2.706$).

Initial inspection of the data revealed the source to be flatter in the low flux states, and steeper in the high states, as observed previously (Miller et al. 2010a). Based upon this, and the previous modeling of the source (Miller et al. 2010a; Lobban et al. 2011) we adopted a simple model of a power law continuum plus neutral scattering gas, all covered with an ionized absorber plus the Galactic column density of neutral gas.

While the ionized absorber is known to be complex and multi-zoned, the lack of soft-band data, and modest spectral resolution of these data prevented us from creating a sophisticated model of that absorbing gas. It was found that a single ionized gas zone was adequate to model the low energy behavior of the source. Thus we fit the 2.0 – 70.0 keV data using a model composed of a power-law continuum, modified by passage through a uniform sphere of ionized gas characterized by an XSTAR model table. For the ionized absorber table we used version 2.1ln11 of the XSTAR code (Kallman & Bautista 2001; Kallman et al. 2004), assuming the abundances of Grevesse & Sauval (1998). XSTAR models the absorbing gas as thin slabs, with parameters of atomic column density and ionization parameter ξ , defined as

$$\xi = \frac{L_{\text{ion}}}{nR^2}$$

Table 2. Reprocessing Model

Observation	N_H^1	N_{PL}^2	N_{Sc}^3	F_{Fe}^4	EW_{Fe}
02+03	$4.75^{+1.25}_{-1.19}$	12.31 ± 0.9	7.06 ± 0.15	2.78 ± 0.74	144
05	$6.28^{+2.12}_{-2.50}$	7.84 ± 0.66	6.72 ± 0.15	4.82 ± 0.11	347
06	$12.75^{+1.95}_{-4.11}$	6.91 ± 0.52	5.05 ± 0.10	1.67 ± 0.65	191
08	$2.70^{+0.80}_{-0.70}$	17.33 ± 1.17	6.86 ± 0.15	3.58 ± 0.75	125

Note. — ¹ Column density of the ionized absorber in units of $10^{22} \text{ atom cm}^{-2}$. ² Power-law normalization at 1 keV, in units $10^{-3} \text{ photons cm}^{-2} \text{ s}^{-1}$. ³ The normalization of the scattered continuum component at 1 keV, in units $10^{-2} \text{ photons cm}^{-2} \text{ s}^{-1}$. ⁴ The Fe K emission line normalization is given in units $10^{-5} \text{ photons cm}^{-2} \text{ s}^{-1}$. In the fit, photon index, the ionization of the absorber and the column density of the scattering gas were consistent with the same values for all observations and were therefore linked in the fit. This yielded: $\log \xi = 2.31 \pm 0.02$, $\Gamma = 2.33 \pm 0.05$ and a column density of the neutral scattering gas $N_H = 6.0 \pm 3.1 \times 10^{24} \text{ cm}^{-2}$. A reprocessed Fe K α emission line complex was allowed in the fit, with column and inclination fixed to those of the scattering gas. $\chi^2_r = 1.06/537$ dof. Errors are calculated at 90% confidence.

that has units erg cm s^{-1} and where L_{ion} is the ionizing luminosity between 1 and 1000 Rydbergs, n is the gas density in cm^{-3} and R is the radial distance (cm) of the absorbing gas from the central continuum source. The spectral energy distribution was taken to be a simple power law with $\Gamma = 2.5$. Following Lobban et al. (2011) the turbulent velocity was taken as $\sigma = 200 \text{ km s}^{-1}$.

The neutral scattering reprocessor gas was modeled using the toroidal reprocessor model, MYTORUS (Murphy & Yaqoob 2009; Yaqoob et al. 2010). The torus has a circular cross section, whose diameter is characterized by the equatorial column density, N_H . The torus is illuminated by a central X-ray continuum. The torus is assumed to have an opening angle (half angle) of 60° , and this corresponds to a global covering factor of 50% (and a solid angle subtended by the structure at the central X-ray source of 2π steradians). The MYTORUS model self-consistently calculates the Fe K α and Fe K β fluorescent emission lines in a separate table to the opacity profile and the scattered spectrum. The availability of these components of reprocessing in separate tables allows the use of the so-called “decoupled mode”, whereby one can allow the scattered, line emission and opacity tables to vary independently, to allow for time delays between direct continuum, Compton-scattered continuum, and fluorescent line photons. All tables include the effects of Compton scattering. The element abundances for MYTORUS are solar (Anders & Grevesse 1989) and the photoelectric absorption cross-sections are those of Verner et al. (1996). Our model included only the scattered spectrum and line emission component. Our fits assumed an inclination angle of 0° for MYTORUS, representative of a face-on scattering torus, with the reprocessing matter out of the direct line-of-sight.

This simple model provided a good fit to all of the flux states exhibited by NGC 4051 (Fig. 1, Table 2). The neutral scattering gas yielded column density $N_H = 6.0 \pm 3.1 \times 10^{24} \text{ cm}^{-2}$; with our model construction, this column density is that inferred for the scatterer only and not associated with the direct transmitted continuum. The emission line component of MYTORUS has been converted to Fe K α line fluxes and equivalent widths for ease of interpretation of the tabulated fits.

The data are consistent with a constant column density for the scattering gas, and column variations for the ionized absorber such that in the high state, the column of the ionized gas is low. Other variations, such as the ionization state or covering fraction of the absorber cannot be ruled out using these data, so our fits provide only a simple parameterization of that aspect of the source behavior.

Fitting all the *NuSTAR* spectra simultaneously with a single spectral model (ie not allowing any spectral variation between

epochs, so we could obtain the mean scattering fractions), we found the scattered X-ray component (including Fe K line) provides a fraction (of scattered to total flux in each band) < 0.14 , 0.17 ± 0.08 , 0.25 ± 0.08 and 0.55 ± 0.10 of the total flux in the 2-4.0, 5.0-7.5, 8-15 and 15-70 keV bands, respectively. The mean spectral model is shown in Fig. 2.

5 MEASUREMENT OF THE X-RAY TIME-DELAY TRANSFER FUNCTION

To measure time delays between bands of differing photon energy, we adopt the method described by Miller et al. (2010a,b). We first create time series in two broad photon energy bands, then use a maximum likelihood method to fit a joint model to the power spectral density (PSD) in the two bands and to the cross-spectral density, fitting to the data autocorrelation in the time domain. Time delays as a function of temporal frequency are obtained from the phases of the cross-spectral density. The method rigorously accounts for gaps in the timing data and allows accurate estimates of statistical uncertainties in PSD, cross-spectral density and time delays, including estimation of the covariance between the measured values if required. The method has been independently coded and tested by (Zoghbi et al. 2013).

In this paper, given the very broad bandpass afforded by the *NuSTAR* observations, we have measured the time delays between pairs of four energy bands: 2–4 keV, 5–7.5 keV, 8–15 keV, 15–70 keV. Note that each observed photon in these energy bands is given equal weight in the analysis, such that, in the absence of significant background flux, the optimum signal-to-noise ratio is obtained in the analysis, irrespective of the source spectrum or the instrument spectral response. Note that, although the best available photon calibration has been applied, inaccuracies in photon energy calibration have little effect on the results in these broad energy bands, and the analysis does not make use of knowledge of the instrument’s spectral response. However, the source spectrum and the instrumental spectral response should be considered when interpreting the results (for example, although the highest energy band extends to 70 keV, the results are completely dominated by photons from the lower end of the bandpass around 15 keV).

The ‘lag spectra’ of time delays in four pairs of bands are shown in Fig. 3. The points with error bars show the results from the data analysis, the solid curve depicts a simple model which will be described in section 6. The horizontal bars on each point show the range of temporal frequency covered, the vertical bars indicate the statistical uncertainty in the measured values. In these spectra, we follow the convention that a delay of the higher energy band with

respect to the lower energy band has a positive sign. Thus in all pairs of energy bands, the harder band consistently lags the softer band at temporal frequencies around 5×10^{-5} Hz. The largest time delays have values around 1000 s, but some negative delays are also measured with amplitudes as large as 400 s. Note that lags that are consistent with zero, or with being slightly negative, are observed at the lowest frequencies in some combinations of energy bands, as found also in low states of NGC 4051 by [Alston et al. \(2013\)](#) and as seen in general in the study of [De Marco et al. \(2013\)](#). Note also the very sharp negative features visible in the upper panels of Fig. 3, with marginal evidence for such a feature also in the lower left panel, at frequencies around $2 - 4 \times 10^{-4}$ Hz. These sharp negative features will be discussed further in section 6.

6 DISCUSSION

6.1 A simple transfer function model

In a time delay analysis such as presented in section 5, it is essential to jointly consider the full set of energy bands being analysed and the full set of temporal frequencies. This is particularly important when, as seen here, sharp features are seen in the frequency domain. There could be a number of possible interpretations of such sharp features.

First, they could be considered to be a genuinely narrow-band phenomenon that is independent of any features that may appear at other frequencies. Such a mode may exist, however to date no physical model for such a narrow-band time delay feature has been proposed in the literature. We note that if a feature is narrow in frequency, then it must be extremely broad in the time domain, and such a feature is not generally consistent with the expectations of reverberation models in which delayed reflection is seen from material covering a narrow range of distances from the primary X-ray source.

An interpretation more commonly proposed is that there are two separate origins for the positive and negative lags. In this case, the low frequency positive lag arises from the inward propagation of accretion disk fluctuations: changes in harder bands emitted from close-in are delayed with respect to softer bands from further out. The higher-frequency negative lag results from ionized reflection from the inner accretion disk, whereby the soft band lags the hard as a result of the greater contribution of the reflected spectrum below 1 keV, compared to a harder continuum reference band (e.g. above 2 keV). The combination of these two phenomena is then suggested to give the oscillatory nature of the lag spectrum (positive followed by negative lag vs frequency). Such a hybrid model was proposed for the negative lags observed in 1H 0707–495 by [Fabian et al. \(2009\)](#) and [Zoghbi et al. \(2010\)](#), and it was proposed that the strong soft-band reflection contribution (causing the soft-band lag, i.e. the negative lag) arose from an anomalously large excess of Fe L emission in the accretion disk at energies below 1 keV, caused by super-solar (by a factor 11) abundance of iron. However, such an explanation does not provide a viable model for the NGC 4051 data as the softer reference bands (2–4 keV, 5–7.5 keV or even 8–15 keV vs 15–70 keV) have a much lower fraction of reflected/scattered X-rays compared to the hardest (15–70 keV) band, where most of the Compton hump is apparent (Fig. 2).

Another problem with the hybrid models is that temporal features should not be considered to be independent quantities. Time delays arising at one frequency can give features that appear at another frequency in lag spectra (and other temporal analysis prod-

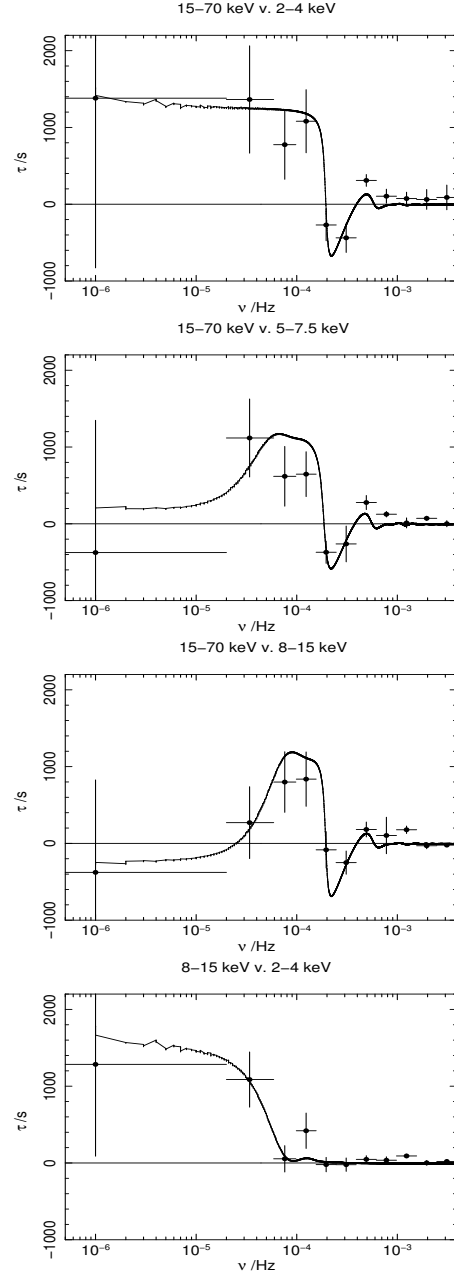


Figure 3. Broadband time delay spectra of NGC 4051 from the archived *NuSTAR* data, shown by the points with error bars, together with a jointly-fitted model using the transfer function described in the text (solid line). The panels show delays measured between 2–4 keV & 15–70 keV (upper left), 5–7.5 keV & 15–70 keV (upper right), 8–15 keV & 15–70 keV (lower left) and 2–4 keV & 8–15 keV (lower right).

ucts). The time domain response function may contain sharp temporal transitions, for example, caused by having a finite range of time delays in a reverberation model, that result in oscillations and negative features in the frequency domain, as proposed by [Miller et al. \(2010b\)](#); [Miller & Turner \(2011\)](#).

A significant cause of the lack of consensus to date on the most likely physical explanation is that measurement of the relative time delay between energy bands by a cross-correlation technique does not reveal whether the time lag arises in one band or the other, or in some combination of the two. One analysis of particular relevance

to this issue was made by [Legg et al. \(2012\)](#): there, the time series in individual energy bands for three AGN, including the *Suzaku* observations of NGC 4051 (section 2), were analysed assuming a ‘moving average’ model for the response function. In one AGN in particular, Ark 564, a very clear response function was obtained showing a sharp-edged response function extending a few ks after the primary flares in emission at energies above 4 keV, with no evidence for such a response at lower photon energies. So in Ark 564 we measured the reverberation directly, as a lag in the hard band, not the soft ([Legg et al. 2012](#)). The sharp negative lag in Ark 564 arises from a sharp-edged temporal response function in the hard band ([Legg et al. 2012](#)). Such an explanation is well-suited to the sharp negative feature seen in the present data for NGC 4051¹, as it arises in multiple combinations of energy bands, not only those that might contain a particular spectral feature.

To illustrate the ability of the latter model to fit the NGC 4051 *NuSTAR* results, we have fitted approximately a simple top-hat response function jointly to the time lags in sets of three pairs of energy bands. The model follows that discussed for 1H0707-495 by [Miller et al. \(2010b\)](#). In each band, the response function comprises a delta function at the time origin, corresponding to a contribution from unscattered (direct) emission, plus a top-hat delayed function with a minimum and maximum time delay. For this illustration, the 2 – 4 keV band was assumed to comprise only direct light with no scattered component. In the remaining energy bands, the ratio of the flux in the direct and scattered components was a free parameter, as was the maximum time delay in the response function. The minimum time delay was also a free parameter but was the same for all energy bands: thus in fitting to any three energy bands there were a total of 5 free parameters. The best-fit was obtained by minimising the total χ^2 between the model and the data points shown in Fig. 3, ignoring for this illustration the effect of covariance between the measured time delay values. The model-fitting was repeated for differing combinations of three of the four energy bands used in our analysis and consistent results were obtained. The best-fit model is shown in Fig. 3, where it may be seen that it provides a good description of the time delay behaviour as a function of frequency in all four pairs of energy bands, at frequencies below about 5×10^{-4} Hz, including a good description of the sharp negative delay feature around $2 - 4 \times 10^{-4}$ Hz and the variations seen in the observed delays between the pairs of energy bands at the lowest frequencies. The model does not reproduce the small residual lags seen at higher frequencies, particularly in the cross-correlation between the 2 – 4 and 15 – 70 keV bands, and it is expected that a more complex model would be needed to reproduce those features, as discussed by [Miller et al. \(2010b\)](#). In particular, the variations in the hardest X-rays appear to be delayed by about 100 s with respect to soft X-ray variations at the highest frequencies, which might arise from Compton scattering delays within a scattering region, possibly even associated with the primary X-ray continuum generation. We regard the success of this simplest of possible models in explaining the gross time delay properties as strongly indicative of the power of this interpretation of the lag spectra. We do not expect that such a simple model will be correct in detail - the model discussed in this section is indicative only - but it does show how the most obvious features in the lag spectra may have a common origin in all the energy bands over the full energy range of the *NuSTAR*

Table 3. Parameters of the best-fit top-hat response function. For each energy band in column 1, the minimum time delay (column 2), maximum time delay (column 3) and fraction of scattered light, R (column 4) are given.

band	t_{\min}/s	t_{\max}/s	R
2-4 keV	-	-	0
5-7.5 keV	2200	14400	0.14
8-15 keV	2200	10600	0.22
15-70 keV	2200	2900	0.47

data - and that, as seen in Ark 564, sharp negative lags may arise without any delayed response in the softest energy band.

6.2 A simple light echo model for NGC 4051

The above simple top-hat model may be viewed as a conveniently simple mathematical model of the response function, without any particular physical interpretation being implied. However, the top-hat model does have a simple interpretation in the context of light echo reverberation models, as we now discuss.

A top-hat temporal response function arises in the case of scattered emission from a uniform, isotropic, thin shell surrounding a central source, where the maximum time delay in the response function is given by the light travel time across the diameter of the shell. A minimum time delay that is greater than zero may arise if scattered light close to the line of sight is absent, such as might be caused either by holes in the scattering distribution, or by the scattering being caused by illuminated surfaces that, along the line of sight, face away from the observer.

The parameters of the best-fit model from Section 6.1 are shown in Table 3. It may be seen that the fraction of scattered light, R , increases with increasing energy, as expected in the scattering of X-rays from absorbing material, either an accretion disk or more general circumnuclear material (e.g. [Miller & Turner 2013](#)). These scattered fractions are consistent with those found from the spectral model (Section 4).

As photon energy increases, the fraction of scattered light increases but the maximum time delay decreases (Table 3). This behaviour could be achieved if soft photons that are scattered at small radii are rapidly absorbed, whereas soft photons scattering from larger radii survive. In contrast, hard photons must be scattered from small and large radii. This could be achieved in a multi-layered system of partially-covering, scattering clouds, in which the optical depth through clouds close to the primary X-ray source is high, such that only high energy photons may escape the scattering region, whereas a smaller fraction of lower energy photons that escape the inner regions may then be scattered from larger radii and survive. A schematic diagram illustrating this possibility is shown in Fig. 4 (in the context of this schematic, the tabulated scattered component in Section 4 represents the total scattered hard X-rays from both white and gray clouds). A compelling physical interpretation of this simple picture is that of reprocessing in a stratified wind: if the wind density profile drops off more steeply than r^{-2} then the ionization of the wind would increase with radial distance, which would result in the harder X-rays preferentially scattering from the denser, low ionization inner gas. Such a wind would need clumps however, to be consistent with the top hat function, whose minimum timescale does not extend down to zero.

The scattered fractions observed in these data (Table 3) are consistent with those of [Miller & Turner \(2013\)](#). In those models, continuum emission from the primary source is suppressed by partial covering of material with geometrical covering fraction around

¹ We note that the *Suzaku* data for NGC 4051 were of insufficient quality to reveal any sharp features in the lag spectrum, although the *XMM* data analysed by [Alston et al. \(2013\)](#) did detect negative lags.

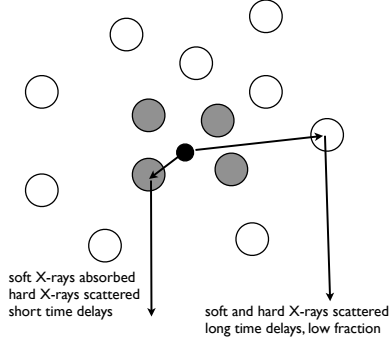


Figure 4. Schematic diagram illustrating how the energy-dependent time delays inferred for NGC 4051 might arise from a multi-layered distribution of scattering clouds around a central source.

50 percent that has a high optical depth to Compton scattering, that emission is replaced by time-delayed scattered light from the illuminated surfaces of the circumnuclear material. Clearly, the current observations and analysis are incapable of definitively testing such a simple model, but future modelling may be able to provide testable predictions of the light echo scenario. We make one final note here, that the light echos expected from the [Miller & Turner \(2013\)](#) models may also predict an excess of delayed emission in the ‘red wing’ continuum region at energies below Fe K, as seen in some other AGN (e.g. [Kara et al. 2015](#)).

7 CONCLUSIONS

Timing analysis of five archived *NuSTAR* observations of NGC 4051 show lags between flux variations in different energy bands. The harder band flux variations consistently lag the softer band, with lags of at least 1000 s at temporal frequencies $\sim 5 \times 10^{-5}$ Hz. The data also show negative lags, i.e. soft-photon lags up to amplitudes of 400s at temporal frequencies $\sim 2 \times 10^{-4}$ Hz.

The presence of a soft lag in the cross correlation between bands where the softer energy band should contain little or no scattered light indicates that negative lags do not arise from soft band scattered or reflected light. This argues against an origin of the negative lag as a reverberation signal from the inner accretion disk, as has been suggested for similar timing behaviour observed in other AGN.

Scattering fractions derived from the data indicate the reprocessor to have a global covering fraction $\sim 50\%$ around the nucleus. The scattered fraction of light increases with increasing photon energy. However, the maximum time delay is greater in the softer bands. This indicates that any soft photons that are scattered at small radii are rapidly absorbed, whereas soft photons scattering from larger radii likely survive. A multi-layered ensemble of partially-covering, scattering clouds, could produce such effects, if the optical depth through clouds close to the primary X-ray source were high, such that only high energy photons may escape that scattering region, while a smaller fraction of lower energy photons

that escape the inner regions could then be scattered from larger radii and survive. A clumpy stratified wind is one possible physical model for such a reprocessor.

8 ACKNOWLEDGEMENTS

T.J. Turner acknowledges financial support from NASA grant NNX11AJ57G. J.N. Reeves acknowledges financial support from STFC and from NASA grant number NNX15AF12G. V.B. acknowledges the support from the grant ASI-INAF *NuSTAR* I/037/12/0. This research has made use of data obtained with the *NuSTAR* mission, a project led by the California Institute of Technology (Caltech) and managed by the Jet Propulsion Laboratory (JPL).

REFERENCES

- Alston W. N., Vaughan S., Uttley P., 2013, *MNRAS*, **435**, 1511
 Anders E., Grevesse N., 1989, *Geochim. Cosmochim. Acta*, **53**, 197
 Arévalo P., Papadakis I. E., Uttley P., McHardy I. M., Brinkmann W., 2006, *MNRAS*, **372**, 401
 De Marco B., Ponti G., Cappi M., Dadina M., Uttley P., Cackett E. M., Fabian A. C., Miniutti G., 2013, *MNRAS*, **431**, 2441
 Denney K. D., et al., 2010, *ApJ*, **721**, 715
 Dickey J. M., Lockman F. J., 1990, *ARA&A*, **28**, 215
 Fabian A. C., et al., 2009, *Nature*, **459**, 540
 Grevesse N., Sauval A. J., 1998, *Space Sci. Rev.*, **85**, 161
 Haardt F., Maraschi L., 1991, *ApJ*, **380**, L51
 Kallman T., Bautista M., 2001, *ApJS*, **133**, 221
 Kallman T. R., Palmeri P., Bautista M. A., Mendoza C., Krolik J. H., 2004, *ApJS*, **155**, 675
 Kara E., et al., 2015, *MNRAS*, **446**, 737
 Kaspi S., Netzer H., Chelouche D., George I. M., Nandra K., Turner T. J., 2004, *ApJ*, **611**, 68
 Kotov O., Churazov E., Gilfanov M., 2001, *MNRAS*, **327**, 799
 Krongold Y., Nicastro F., Elvis M., Brickhouse N., Binette L., Mathur S., Jiménez-Bailón E., 2007, *ApJ*, **659**, 1022
 Legg E., Miller L., Turner T. J., Giustini M., Reeves J. N., Kraemer S. B., 2012, *ApJ*, **760**, 73
 Lobban A. P., Reeves J. N., Miller L., Turner T. J., Braitto V., Kraemer S. B., Crenshaw D. M., 2011, *MNRAS*, **414**, 1965
 McHardy I. M., Papadakis I. E., Uttley P., Page M. J., Mason K. O., 2004, *MNRAS*, **348**, 783
 Miller L., Turner T. J., 2011, in *Narrow-Line Seyfert 1 Galaxies and their Place in the Universe*. ([arXiv:1106.3648](#))
 Miller L., Turner T. J., 2013, *ApJ*, **773**, L5
 Miller L., Turner T. J., Reeves J. N., Lobban A., Kraemer S. B., Crenshaw D. M., 2010a, *MNRAS*, **403**, 196
 Miller L., Turner T. J., Reeves J. N., Braitto V., 2010b, *MNRAS*, **408**, 1928
 Miniutti G., Fabian A. C., 2004, *MNRAS*, **349**, 1435
 Murphy K. D., Yaqoob T., 2009, *MNRAS*, **397**, 1549
 Nagao T., Murayama T., Taniguchi Y., Yoshida M., 2000, *AJ*, **119**, 620
 Ponti G., Miniutti G., Cappi M., Maraschi L., Fabian A. C., Iwasawa K., 2006, *MNRAS*, **368**, 903
 Pounds K. A., Reeves J. N., King A. R., Page K. L., 2004a, *MNRAS*, **350**, 10
 Pounds K. A., Reeves J. N., Page K. L., O’Brien P. T., 2004b, *ApJ*, **605**, 670
 Titarchuk L., 1994, *ApJ*, **434**, 570
 Turner T. J., Miller L., Reeves J. N., Kraemer S. B., 2007, *A&A*, **475**, 121
 Uttley P., Cackett E. M., Fabian A. C., Kara E., Wilkins D. R., 2014, *A&A Rev.*, **22**, 72
 Verner D. A., Ferland G. J., Korista K. T., Yakovlev D. G., 1996, *ApJ*, **465**, 487
 Yaqoob T., Murphy K. D., Miller L., Turner T. J., 2010, *MNRAS*, **401**, 411
 Zoghbi A., Fabian A. C., Uttley P., Miniutti G., Gallo L. C., Reynolds C. S., Miller J. M., Ponti G., 2010, *MNRAS*, **401**, 2419

Zoghbi A., Reynolds C., Cackett E. M., 2013, [ApJ](#), **777**, 24

Zoghbi A., et al., 2014, [ApJ](#), **789**, 56